ELSEVIER

Polymer 42 (2001) 9423–9431

polymer

www.elsevier.com/locate/polymer

Isothermal crystallization kinetics and melting behaviour of poly(ethylene terephthalate)

X.F. Lu, J.N. Hay*

Plastic Materials Laboratory, The School of Metallurgy and Materials, The University of Birmingham, Edgbaston, Birmingham, B15 2TT, UK

Received 23 April 2001; received in revised form 30 May 2001; accepted 2 July 2001

Abstract

Differential Scanning Calorimetry has been used to study the isothermal crystallization kinetics and melting behaviour of PET. Kinetic analysis indicated that the overall crystallization of PET involved two processes, attributed to primary and secondary crystallization. Secondary crystallization occurred consecutively with primary and both processes obey different Avrami time dependences. The primary process was that of heterogeneous nucleation and three-dimensional spherical growth that was confirmed by direct observation of spherulites by SEM. Secondary crystallization was that of one dimensional growth involving fibrillar growth between the primary lamellae of the spherulites. Accordingly primary crystallization has a stronger temperature dependence on temperature than secondary. Further analysis based on Hoffman–Lauritzen theory revealed that PET crystallization followed regime I kinetics at temperatures between 490 and 564 K. Below 490 K, regime II kinetics were operational. Multiple endotherms were observed in melting PET and attributed to the effect of crystal perfection and re-crystallization on heating from the crystallization temperature to the m.pt. Increasing the crystallization temperature and the rates of heating during melting scans minimized these effects.

Increases in yield stress, yield strain and decrease in elongation at break with crystallinity were ascribed to the strengthening effect of the crystals on the amorphous matrix, accompanied by the change in mechanism of tensile deformation from ductile yielding to craze-crack growth.

Keywords: Poly(ethylene terephthalate); Isothermal crystallization kinetics; Melting

1. Introduction

Poly(ethylene terephthalate) (PET) is a well established engineering polymer used in the manufacture of fibre, film, tape, mouldings and pressurized liquid containers. As with other semi-crystallisable polymer, the physical and mechanical properties of PET depend on its microstructure and so are determined by crystallization rate, the degree and quality of crystallinity. In order to control the rate of crystallization and the degree of crystallinity and to obtain the desired morphology and properties, a great deal of effort has been made into studying the crystallization kinetics and determining the change in material properties [1–18]. Many experimental techniques have been applied to these studies including calorimetry, dilatometry, infrared spectroscopy, X-ray diffraction, light scattering and others [19]. Differential scanning calorimetry (DSC) in particular has been very successful in studying polymer crystallization kinetics [20–21].

Although PET has been largely studied, it has not been investigated in all aspects of crystallization behaviour, e.g. secondary crystallization, and some studies conflicted with one another [22–23]. This paper aimed to investigate the isothermal crystallization kinetics and mechanism of PET in more detail primarily by using DSC. Relevant to these aspects, the melting behaviour of PET and the effect of crystallinity on tensile properties have also been investigated.

2. Experimental

Commercial PET with a number average molecular weight of 16 kg mol^{-1} and polydispersity of 2.2 was supplied by ICI plc. in sheet form. It was dried in a vacuum oven at 100°C for 12 h before re-moulding. Disc specimens, 3.0 mm in diameter and 1.5 mm in thickness were cut from the dried sheet and used for all DSC studies on melt-crystallization kinetics.

* Corresponding author. Tel.: +44-121-414-4544; fax: +44-121-414-5232.

E-mail address: j.n.hay@bham.ac.uk (J.N. Hay).

0032-3861/01/$ - see front matter
PII: S0032-3861(01)00502-X

A Perkin–Elmer differential scanning calorimeter, DSC-2, interfaced to a PC computer was used to follow the variation of the rate of heat evolution with time. The temperature scale of the DSC was calibrated from the melting point of high purity metals (99.999%): lead (600.65 K); tin (505.06 K); indium (429.78 K); stearic acid (343.15 K). The power response of the calorimeter was calibrated from the enthalpy of fusion of indium [24], taken to be 28.47 J g^{-1}. Samples were weighted and enclosed in aluminum pans and an empty aluminum pan was used as reference.

All crystallization rate studies were carried out on completely amorphous samples. Corresponding to the different routes to crystallization temperature the samples were heated from the glass or cooled from the melt, isothermal crystallization was referred to as cold- and hot-crystallization, respectively. Isothermal cold-crystallization studies were carried out in the temperature range of 390–410 K. The samples were placed in DSC at 320 K and heated to the desired temperature at 160 K min^{-1}. They were kept at the crystallization temperature for sufficient time that the DSC trace returned to the calorimeter baseline. Isothermal hot-crystallization experiments were performed in the temperature range 480–500 K. For experiments carried out on molten materials, the samples were cooled from above the observed melting point at a rate of 160 K min^{-1} to the crystallization temperature and kept at that temperature until the DSC trace returned to the calorimeter baseline. Each result is an average of three.

A potassium hydroxide solution in methanol was used to etch the surface of crystallized PET. The morphology of the etched specimens was examined on a Jeol, model 5410, scanning electron microscope (SEM).

Tensile load-extension experiments were carried out using an Instron floor standing tester, model TT-BM. Dumbell shaped samples were cut from compression-moulded plaques. The specimens had a gauge length of 25 mm, width 4 mm and thickness 0.8 mm. The cross-head speed was 0.01 cm min^{-1}min with an accuracy of ±1%. The tests were conducted in a constant room at 295 ± 1 K and constant humidity of 50 ± 1%. The applied loads were calibrated by standard weight and an interfaced PC computer recorded the response of samples to the applied load.

3. Results and discussions

3.1. The crystallization of PET

The isothermal crystallization exotherms of PET, obtained as described above, are shown in Figs. 1 and 2. The weight fraction crystallinity, X_t, was obtained from the ratio of the area of the endotherm upto time t divided by the total endotherm, i.e.

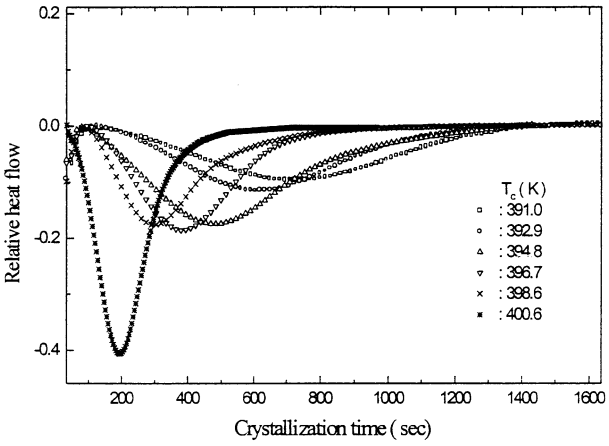

Fig. 1. DSC exotherms of the isothermal cold-crystallization of PET.

$$X_t = \frac{\int_0^t (dH/dt)\, dt}{\int_0^\infty (dH/dt)\, dt} \quad (1)$$

where dH/dt is the heat flow rate. The development of the weight fraction crystallinity with time for cold- and hot-crystallization of PET is shown in Figs. 3 and 4. All isotherms exhibited a sigmoid dependence with time. The dependence of the overall crystallization rate on temperature can be seen from the half-lives in Fig. 5. The dependence of the overall crystallization rate on temperature can be seen from the variation in the half-lives in Fig. 5. This followed the conventional bell-shaped curve with the fastest rate of crystallization in the region of 430–450 K.

A slow increase of crystallinity with time after most of the crystallization had taken place was observed and this was attributed to the presence of secondary crystallization [21,25]. The time dependence was analysed assuming the presence of two crystallization processes, primary and secondary, and using a modified Avrami equation [26] for

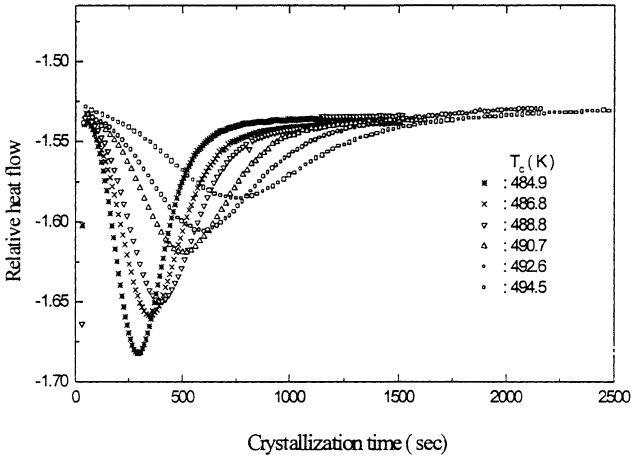

Fig. 2. DSC exotherms of the isothermal hot-crystallization of PET.

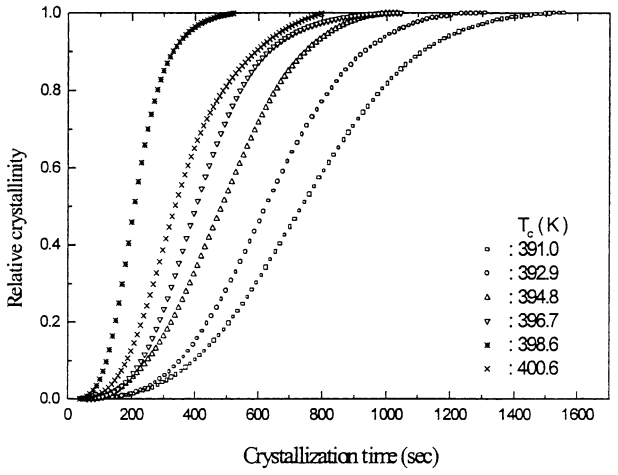

Fig. 3. Development of crystallinity with time during cold-crystallization.

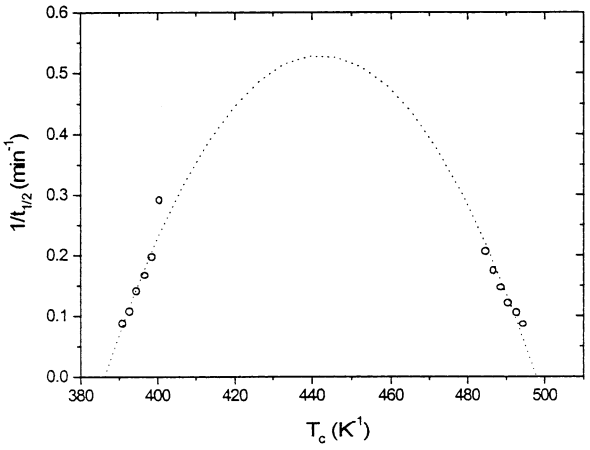

Fig. 5. The overall crystallization rate of PET as a function of crystallization temperature.

which

$$X_t = X_{p,\infty}[1 - \exp(-Zt^n)] \quad (2)$$

where X_t and $X_{p,\infty}$ are the fractional extent of crystallinity at time t, and at the end of the primary process. Z is the primary composite rate constant and n a constant whose value varies according to the primary crystallization mechanism.

Eq. (2) can be differentiated and rearranged to give the n value for the primary process,

$$n = -t\left(\frac{dX_t}{dt}\right)\Big/\left[(X_{p,\infty} - X_t)\ln\left(1 - \frac{X_t}{X_{p,\infty}}\right)\right] \quad (3)$$

Eq. (3) reflects instantaneous values of n as a function of crystallinity, X_t. Empirically, the primary and secondary crystallization processes have been considered to occur either consecutively or concurrently but the n value will predict the change from primary to secondary [26,27]. The resolution of the two processes becomes that of determining a critical value of $X_{p,\infty}$ which marks the completion of the primary crystallization. This was achieved by adjusting $X_{p,\infty}$ until the value of n remains essentially constant at the end of the primary process.

Instantaneous variation in n value with extent of crystallinity is shown typically in Fig. 6. It can be seen that the Avrami exponent changed progressively from 0.5 to 2.6 during the initial development of crystallinity, but remained at 2.6 ± 0.2 over the range 30–90% of the process. Beyond 90%, it suddenly rose towards 4.0 implying the mechanism of crystallization changed beyond the transition point corresponding to the end of the primary process, i.e. at $X_{p,\infty}$. The values of $X_{p,\infty}$ for cold- and hot-crystallization at different temperatures were obtained in this manner and are shown in Table 1.

For cold-crystallization, $X_{p,\infty}$ decreased with increase in temperature, and at the same time the rate constant of primary crystallization increased. For the hot-crystallization of PET, $X_{p,\infty}$ increased with the increasing temperature, and the rate constant of primary crystallization decreased. It would appear that a faster primary crystallization process was accompanied with an increase in the amount of secondary crystallization present.

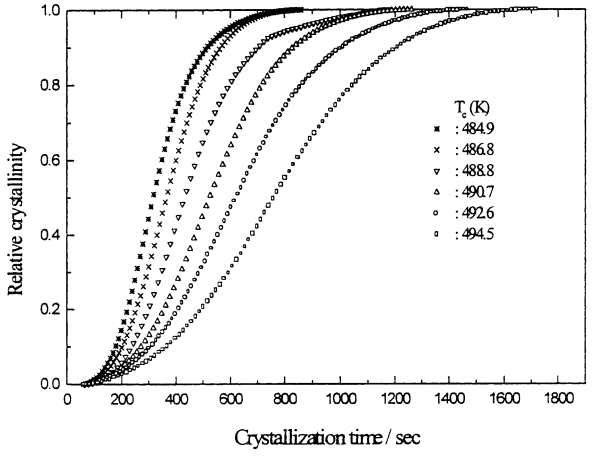

Fig. 4. Development of crystallinity with time during hot-crystallization.

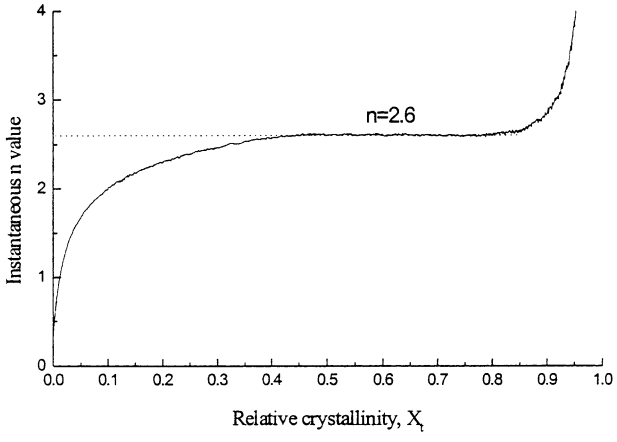

Fig. 6. Variation in n value during PET isothermal crystallization.

Table 1
$X_{p,\infty}$ for PET isothermal crystallization

Cold-crystallization		Hot-crystallization	
Temperature (K)	$X_{p,\infty}$	Temperature (K)	$X_{p,\infty}$
391.0	0.98	484.9	0.91
392.9	0.97	486.8	0.95
394.8	0.96	488.8	0.92
396.7	0.93	490.7	0.95
398.6	0.95	492.6	0.96
400.6	0.91	494.5	0.97

3.2. Primary crystallization

The Avrami kinetic analysis of the primary crystallization process is shown in Figs. 7 and 8 for cold- and hot-crystallization respectively. A series of straight lines were obtained from plots of $(-\ln(1 - [X_t/X_\infty]))$ against $\ln(t)$ for which the slope is equal to the Avrami exponent, n_1 and the intercept at $\ln(t) = 0$ is $\ln(Z_1)$. Values of n_1, Z_1 and the corresponding half-life, $t_{1/2,1}$ for cold- and hot-crystallization are listed in Tables 2 and 3, respectively.

It can be seen from Tables 2 and 3 that the n values were essentially constant at 2.6 ± 0.2 for both cold- and hot-crystallization and are not the integer values required by the crystallization mechanisms considered by Avrami. The values are consistent with other polymer crystallization kinetic studies for which the mechanism is one of growth of spherulites from heterogenious nuclei. Indeed, a spherulitic morphology was observed by SEM in these crystalline samples after etching with methanolic KOH, see Fig. 9.

3.3. Secondary crystallization

Many research workers [28–30] have attributed the deviation to the presence of a secondary process. However, up to now, the exact mechanism of the secondary crystallization has not been clear, thus the analysis of secondary crystallization has been based on certain approximations.

Following Hillier's two-stage crystallization of spherulites in which secondary crystallization develops within the boundaries of the spherulite, Verhoyen and coworkers [31] consider that the secondary crystallization occurs well after the primary has stopped and the two follow their own Avrami kinetic equation.

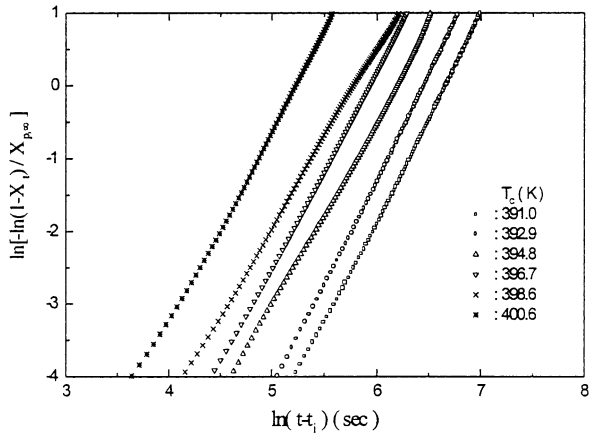

Fig. 7. Avrami analysis for the primary stage of cold-crystallization of PET.

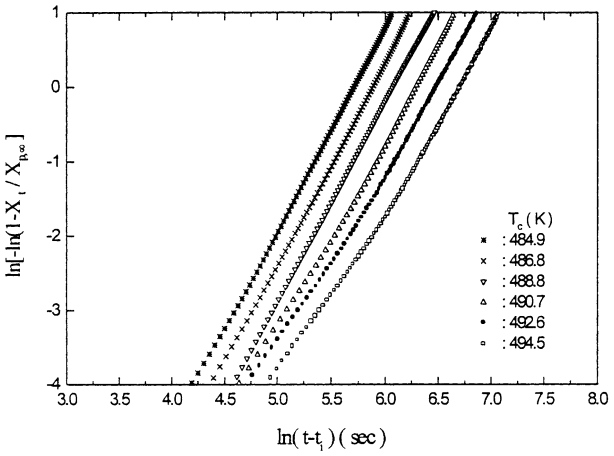

Fig. 8. Avrami analysis for the primary stage of hot-crystallization of PET.

Thus for the primary crystallization,

$$X_p = w_1[1 - e^{-Z_1(t-t_{0,1})^{n_1}}] \quad (4)$$

where $t_{0,1}$ is an induction time for the primary crystallization, and Z_1 and n_1 represent the Avrami constant and rate constant, respectively.

For the secondary crystallization,

$$X_s = w_2[1 - e^{-Z_2(t-t_{0,2})^{n_2}}] \quad (5)$$

where $t_{0,2}$ is the induction time for the secondary crystallization. The essential and necessary condition for the model is $t_{0,2} \gg t_{0,1}$. n_2 and Z_2 represent the Avrami constant and rate constant of the secondary process, respectively. w_1 and w_2 represent the relative importance of the two processes and $w_1 + w_2 = 1$. The total crystallinity developing with time is thus given by

$$X_t = w_1[1 - e^{-Z_1(t-t_{0,1})^{n_1}}] + w_2[1 - e^{-Z_2(t-t_{0,2})^{n_2}}] \quad (6)$$

This equation was used to analyse the crystallization of PET in this study. The relative importance of the two processes, w_1 and w_2, is reflected by the relative degree of crystallinity at the end of primary crystallization, $X_{p,\infty}$, and the secondary process, $X_{s,\infty}$, respectively. An additional assumption was made that the secondary process started at the end of the primary process. Thus, $t_{0,2}$ was set as the time

Table 2
The Avrami rate parameters for PET (Primary stage of cold-crystallization)

T_c (K)	391.0	392.9	394.8	396.7	398.6	400.6
$n_1 \pm 0.1$	2.6	2.5	2.6	2.7	2.6	2.5
$Z_1 \times 10^3$ (min^{-n_1})	1.24	2.66	5.19	7.24	18.6	68.0
$t_{1/2,1}$ (min)	11.4	9.26	6.57	5.42	4.25	3.45

Table 3
Avrami rate parameters for PET (Primary stage of hot-crystallization)

T_c (K)	484.9	486.8	488.8	490.7	492.6	494.5
$n_1 \pm 0.1$	2.7	2.7	2.7	2.5	2.4	2.4
$Z_1 \times 10^3$ ($\min^{-n_1}$)	12.6	7.99	4.75	4.20	3.49	2.71
$t_{1/2,1}$ (min)	4.41	5.22	6.33	7.71	8.72	10.1

Table 4
Avrami rate parameters for PET (Secondary process of cold-crystallization)

T_c (K)	391.0	392.9	394.8	396.7	398.6	400.6
$n_2 \pm 0.1$	1.3	1.3	1.2	1.2	1.2	1.2
Z_2 ($\min^{-n_2}$)	0.17	0.25	0.28	0.32	0.39	0.48
$t_{1/2,2}$ (min)	4.1	3.3	2.5	2.2	1.8	1.5

when the primary process finished and the secondary process started.

The total crystallinity at time, t, has two time dependences, i.e. initially when, $X_t < X_{p,\infty}$,

$$X_t = X_p = X_{p,\infty}[1 - e^{-Z_1(t-t_{0,1})^{n_1}}] \quad (7)$$

and when, $X_t > X_{p,\infty}$,

$$X_t = X_{p,\infty} + X_s = X_{p,\infty} + X_{s,\infty}[1 - e^{-Z_2(t-t_{0,2})^{n_2}}] \quad (8)$$

The cold- and melt-crystallization rates were analysed in terms of these two regions and the kinetic parameters of the secondary crystallization, i.e. the Avrami constant, n_2, rate constant, Z_2, and the half-life, $t_{1/2,}$ obtained. These are listed in Tables 4 and 5, respectively.

From Tables 4 and 5 it can be seen that the n_2 values were about 1.2, suggesting that one dimensional crystal growth is occurring in the final stage of the crystallization. The values of Z_2 and $t_{1/2}$ are dependent on temperature and changing in the same relative way as the values for primary crystallization. In the temperature region of cold-crystallization, the rate of the secondary process decreased with decreasing temperature consistent with the increase in melt viscosity as the glass transition is approached. In the temperature region of hot-crystallization, the rate constant decreased with increasing temperature consistent with nucleation control of crystallization.

Secondary crystallization develops after 90% of the crystallization process has taken place and the kinetic analysis is severely restricted by the limited sensitivity of the DSC. Secondary crystallization continues to develop well beyond the detectable limit of heat flow measurements in the DSC and this reduces the accuracy of determining the rate constants and n value.

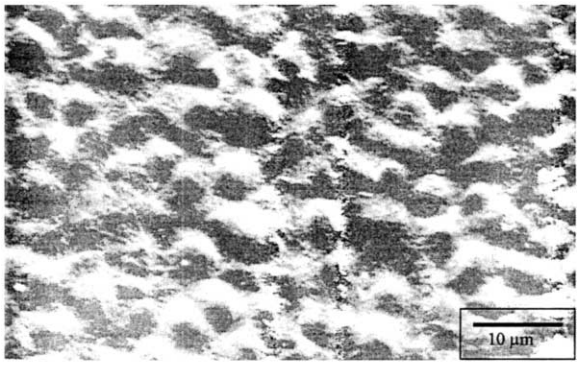

Fig. 9. Spherulites of PET after crystallization at 120°C for 1 h and KOH etching.

3.4. Nucleation characteristics

The crystallization characteristics of thin films of PET were studied by hot stage microscopy. Resolvable spherulites were observed in the temperature range 110 to 160°C. The radii of the spherulites were observed to grow linearly with time up to impingement and the nucleation density was measured from the number of spherulites in the field of view. Radial growth rates increased and nucleation densities decreased with crystallization temperature in the range of cold-crystallization, as can be seen in Fig. 10. Nucleation was heterogeneous as the spherulites reformed in same place within the PET sample on melting and crystallization. Heterogeneous nuclei are most likely to form on a range of different size particles with progressively smaller ones becoming effective with decreasing temperature. The density of nuclei should increase with decreasing crystallization as the more numerous small particles become activated.

3.5. Melting and the equilibrium melting point

In order to understand the temperature dependence of the crystallization rates it was important to measure the equilibrium melting temperature of PET by establishing the rate dependence on the degree of super-cooling, $\Delta T = T_m - T_c$. As described above, PET can be crystallized over a wide temperature range between the glass transition and the melting point. The different thermal history leads to different morphologies as evidenced by the presence of multiple melting endotherms [32–35]. A weak dependence of melting point on crystallization temperature is then observed as a result of melting and re-crystallization or annealing of the sample during the heating to the melting point. This produces further structural changes within the sample. In investigating the effect of heating rate on this recrystallization and subsequent changes in melting behaviour, PET was

Table 5
Avrami rate parameters for PET (Secondary process of hot-crystallization)

T_c (K)	484.9	486.8	488.8	490.7	492.6	494.5
$n_2 \pm 0.1$	1.2	1.3	1.2	1.0	1.3	1.3
Z_2 ($\min^{-n_2}$)	0.28	0.24	0.22	0.18	0.16	0.15
$t_{1/2,2}$ (min)	2.4	2.8	3.2	3.8	4.3	4.7

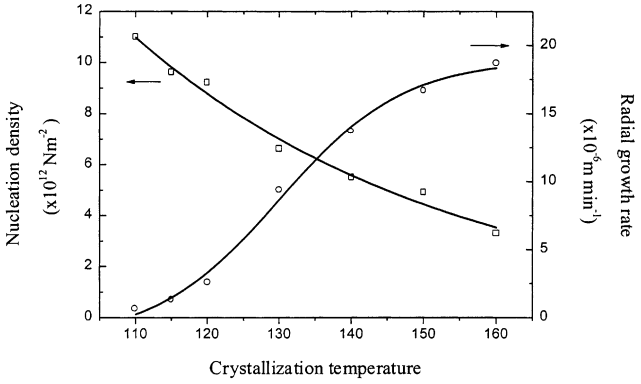

Fig. 10. Changes in nucleation density and crystal growth rate with temperature.

isothermally hot crystallized at 485 K for various periods up to complete crystallization. The samples were then melted at different heating rates from 5.0 to 20 K min^{-1}. Three melting endotherms were observed in these samples, as shown in Fig. 11, labelled 1, 2 and 3 with increasing temperature. Endotherm 1 started about 10 K above the crystallization temperature but shifted to increasing temperature with heating rate. If this is due to the melting of the smallest lamellae produced by secondary crystallization and to inter-lamellar growth it should not develop until after the primary stage is complete.

Endotherm 2 was independent of the heating rate and considered to be characteristic of the melting of the crystals formed in the primary crystallization. Endotherm 3 resulted from the melting and recrystallization of endotherms 1 and 2. Accordingly it increased in intensity with the slower heating rates with the greater amount of time for melting and re-crystallization. Increasing the rate of heating during melting minimized the effect of re-crystallization and, for a specific heating rate, re-crystallization is reduced by crystallizing the sample at higher temperatures. Reliable measurement of melting point should only be made by using high crystallization temperatures and rapid melting rates.

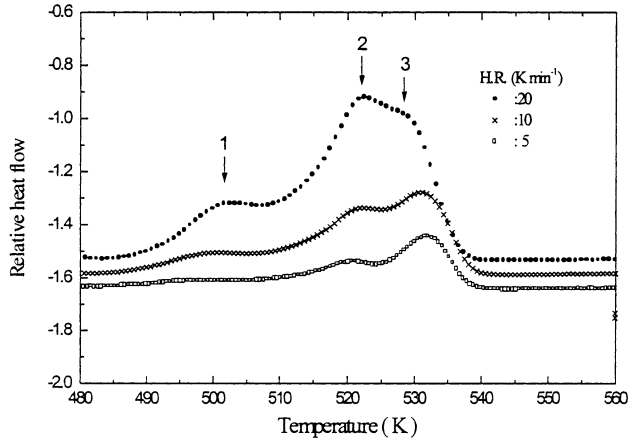

Fig. 11. Effect of heating rate on PET melting behaviour.

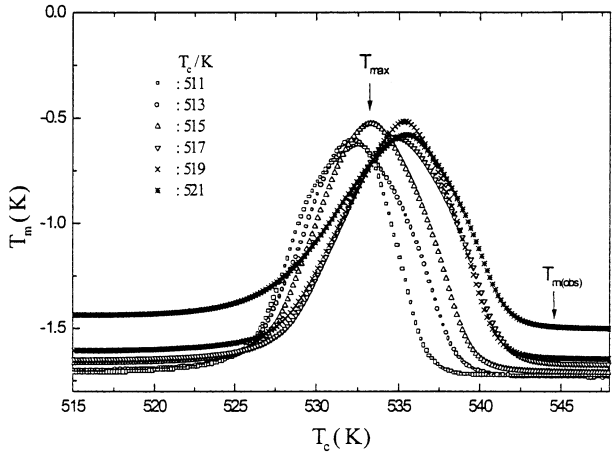

Fig. 12. The development of the melting point on crystallization temperature of PET.

Conventionally the melting point as measured by DSC is defined as the temperature corresponding to the maximum rate of melting, T_{max}. Instead, the temperature corresponding to the last trace of crystallinity of the sample [36] was adopted as $T_{m(obs).}$ Fig. 12 shows the melting endotherms at a heating rate of 20 K min^{-1} of PET isothermal crystallization from 511 to 521 K for 24 h. Further annealing of the samples showed that a stable crystal structure had formed and the observed melting points, $T_{m(obs)}$ did not increase with further increasing time, suggesting that crystal perfection did not occur to any appreciable extent. In addition, a single melting endotherm only was observed and it shifted to higher melting points with the increasing crystallization temperature. The observed melting points were characteristic of the large stable crystals produced at the crystallization temperature.

Using these values, corrected for thermal lag, the procedure suggested by Hoffman et al. [37] was adopted of plotting $T_{m(obs),}$ against T_c to determine the equilibrium melting point, T_m°. The plot was linear, see Fig. 13, and could be interpolated to intersect the line of $T_m = T_c$ at a value for T_m^0

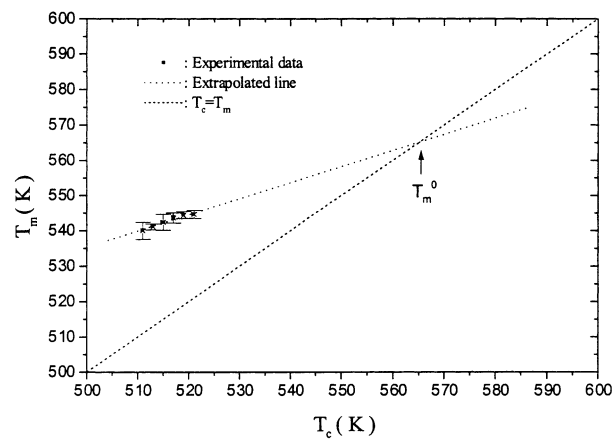

Fig. 13. The determination of the equilibrium melting point.

of 564.0 ± 2.0 K. The slope of the line, i.e. $1/2\beta$ was equal to 0.50 ± 0.1, giving $\beta = 1.0$. This confirmed that no crystal perfection and recrystallization had occurred and caused the thickness of lamellae to increase as PET was further annealed, or while it was being heated during the melting run.

3.6. The temperature dependence of primary and secondary crystallization rates

The primary and secondary crystallization rates at different temperatures were expressed in the form of reciprocal crystallization half-life, $1/t_{1/2}$, using Hoffman–Lauritzen relationship [38] and following Chan and Isayev [39], $(1/t_{1/2})$ and $(1/t_{1/2})_0$ were used to substitute for g and g_0, respectively. The temperature dependence of the crystallization half life $(1/t_{1/2})$ is given by

$$\left(\frac{1}{t_{1/2}}\right) = \left(\frac{1}{t_{1/2}}\right)_0 \exp\left[\frac{-U^*}{R(T-T_\infty)}\right] \exp\left[\frac{-K_g}{T(\Delta T)f}\right] \quad (9)$$

Plots of $\ln[(1/t_{1/2}) + U^*/R(T - T_\infty)]$ against $1/(T\Delta Tf)$ are shown in Fig. 14 for both primary and secondary crystallization. The data is consistent with two linear relationships for both primary and secondary processes, corresponding to two nucleation regimes,

It is considered that at high crystallization temperatures, corresponding to small degrees of super-cooling, regime I kinetics are operative. In this case, surface nucleation involved in crystal growth leads to rapid completion over the surface of the new phase prior to the next nucleation event. Therefore, secondary nucleation dominates crystal growth and for primary and secondary crystallization,

$$K_{g,I} = \frac{4b\sigma\sigma_e T_m^0}{\Delta H_f k} = 5.0 \times 10^5 \text{ K}^2$$

At large degrees of super-cooling, i.e. below 490 K, regime II kinetics are operative, where the rates of the secondary nucleation and the spread of the molecular strip along the growing face are comparable.

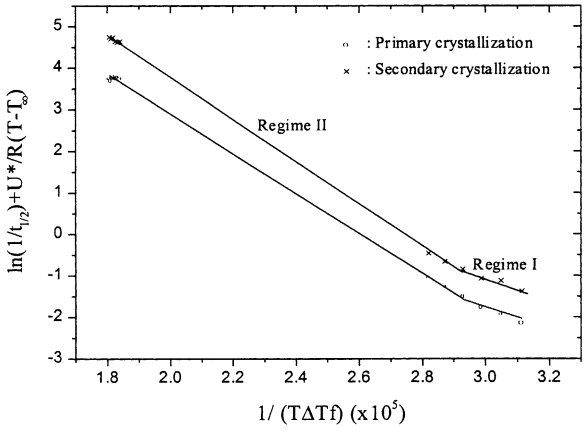

Fig. 14. $[\ln[\ln[(1/t_{1/2}) + U^*/R(T - T_\infty)]$ versus $1/(T\Delta Tf)$.

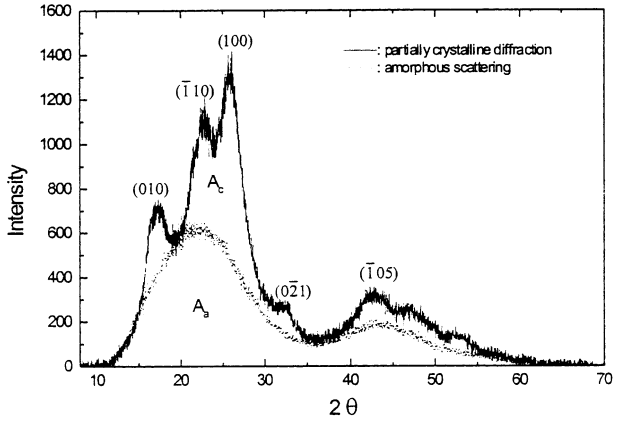

Fig. 15. WAXD diffractograms of 30% crystallized and amorphous PET.

Studies with polyethylene [38,40] also clearly show a defined transition from regime I to II accompanied by a morphology change from axialites to spherulites. PET also exhibits spherulite morphology at low temperature consistent with the regime II kinetics, applicable to PET crystallization at large super-cooling. In this case, the primary and secondary processes have the same K_g value, i.e.

$$K_{g,I} = \frac{2b\sigma\sigma_e T_m^0}{\Delta H_f k} = 2.5 \times 10^5 \text{ K}^2$$

where b is the monomolecular layer thickness, taken to be the perpendicular separation of (010) planes. This is 5.53 Å [41]. σ is the side surface free energy of the polymer crystal, which is often estimated as [38,40,42],

$$\sigma = \partial \Delta H_f (a_0 b_0)^{1/2} \quad (10)$$

Where ∂ was derived empirically to be 0.11 by analogy with the known behaviour of hydrocarbons [43].

The unit cell dimensions, a_0 and b_0 for PET used in the analysis are 4.57 and 5.95 Å, respectively [44]. Accordingly, for PET isothermal crystallization, $\sigma = 1.09 \times 10^{-2}$ J m^{-2} Using $T_m^0 = 564 \pm 2$ K and the recommended

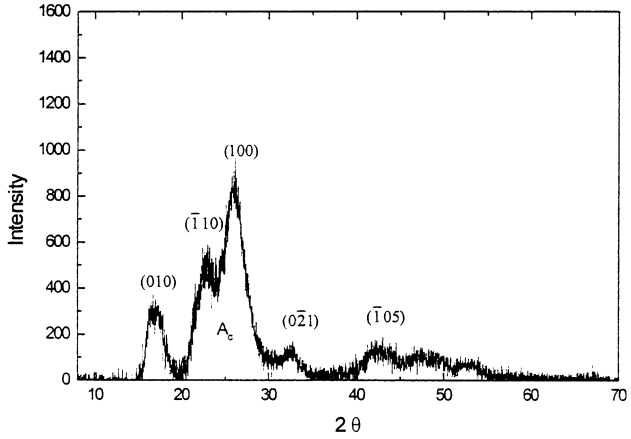

Fig. 16. The crystalline diffractogram of 30% crystallized PET after subtraction of the amorphous background.

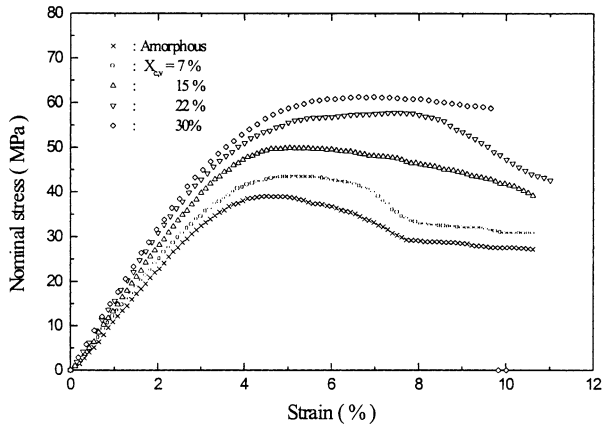

Fig. 17. The stress–strain curves of PET with various degree of crystallinity.

values [38] $U^* = 6284\ \mathrm{J\ mol^{-1}}$ and [5] $\Delta H_f = 2.1 \times 108\ \mathrm{J\ m^{-3}}$ the value of σ_e was obtained as $\sigma_e = 0.106 \pm 0.02\ \mathrm{J\ m^{-2}}$ An alternative method for determining the fold surface free energy, σ_e has been applied by Wlochowicz and Przygocki [45], from small-angle X-ray diffraction to measure the fold period in PET crystal at known melting points. According to the kinetic theory of chain folding [38] they calculated σ_e for PET crystallized in temperature range 427–473 K to be $90.9–93.6 \times 10^{-3}\ \mathrm{J\ m^{-2}}$.

Obviously, the values for σ_e obtained in the present study are in very close agreement with these results, although a very different method was used in their calculation.

3.7. The effect of crystallinity on the tensile properties of PET

PET was annealed at 120°C for different times to produce samples of different degrees of crystallinity and their stress–strain behaviour investigated. WAXS and DSC were used to measure the degree of crystallinity. WAXS measures the volume fraction crystallinity, $X_{c,v}$. The amorphous scattering curve was scaled according to the amorphous content, and the crystalline peaks obtained by subtraction. The ratio of

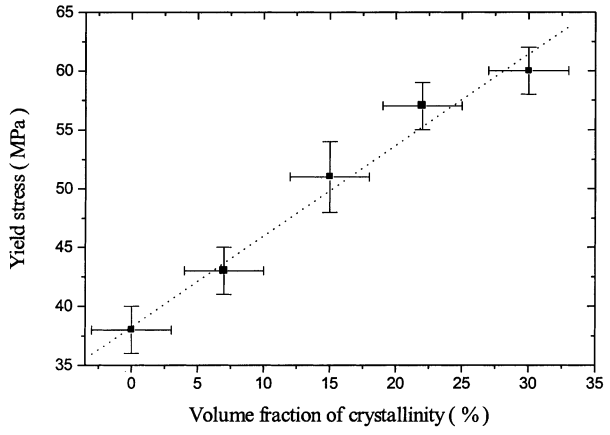

Fig. 18. The relationship between yield stress and crystallinity of PET at 23°C.

Table 6
The effect of crystallinity on the tensile properties of PET (295 ± 1 K at strain rate $4.0 \times 10^{-3}\ \mathrm{min^{-1}}$)

% Crystallinity	Yield stress (MPa)	Yield strain (%)
0	38 ± 2	3.8 ± 0.5
7 ± 3	43 ± 2	4.3 ± 0.5
15 ± 3	51 ± 3	5.3 ± 0.5
22 ± 3	57 ± 2	6.5 ± 0.5
30 ± 3	60 ± 2	7.0 ± 0.5

the area of the crystalline bands, A_c to the total area, $(A_c + A_a)$, as shown in Figs. 15 and 16, was determined and used to define the volume fraction crystallinity, i.e.

$$X_{c,v} = \frac{A_c}{A_c + A_a} \tag{11}$$

These samples were subjected to stress–strain analysis as can be seen in Fig. 17. The tensile characteristics are summarized in Table 6. There was a progressive increase in the strain at yield with increasing crystallinity as well as an almost linear increase in yield stress with crystallinity, see Fig. 18. It would appear that the crystalline phase is reinforcing amorphous regions. However, as the degree of crystallinity increased shape of the neck becomes more diffuse and a region of uniform drawing eventually occurs. At this stage fracture occurs at a lower stain. Crystallization would appear to make PET more brittle as a result of increasing the yield stress and a change in fracture mechanism from ductile shear yielding to craze crack growth.

4. Conclusions

PET isothermal crystallization kinetics, including cold- and hot-crystallization were measured by using DSC. It was observed that the overall crystallization included two different steps i.e. primary and secondary crystallization, and the two occurred consecutively. The two processes were separated at a critical value of the degree of crystallinity, $X_{p,\infty}$, when there was a sudden change in the value of the Avrami exponent, n, from 2.6 to 1.2, consistent with this transition from primary to secondary.

The Avrami analysis indicated that the primary crystallization of PET followed the mechanism of three-dimension spherical growth on heterogeneous nuclei, while the secondary crystallization was linear growth within formed spherulites. The relevant kinetics parameters at various temperatures (390–400 and 480–500 K), for primary and secondary crystallizations were obtained separately.

The study on PET melting behaviour focused on the determination of the equilibrium melting point. The multiple melting peaks were ascribed to crystal perfection and recrystallization as the polymer was further annealed, or while it was being heated during the melting run. The effects of crystal perfection and recrystallization were minimized

by increasing the crystallization temperature as close as possible to the melting point temperature, and by increasing the rate of heating during the melting run. According to Hoffman and Weeks equation, the equilibrium melting point of PET, T_m^0 was determined to be 564 ± 2 K and β was 1.0 ± 0.2. The value of β confirmed there were no further crystal perfection and recrystallization existing during the melting measurements.

Analysis using Lauritzen–Hoffman equation indicated that at temperatures above 490 K, PET crystallization followed regime I kinetics, while below 490 K, regime II kinetics was operative. The fold surface energies, σ_e for PET primary and secondary crystallizations had the same value, 0.106 ± 0.02 J m^{-2}, which was ten times larger than the side surface energy σ.

The increase in the yield stress, and decrease in elongation at break with degree of crystallinity was attributed to the reinforcing effect of crystalline regions on the amorphous matrix, while there was a gradual change in mechanism of tensile deformation from ductile shear yielding to craze-crack growth with the increasing crystallinity.

Acknowledgements

We would like to thank Mr Frank Biddlestone for technical support. X.F.L. acknowledges the award of an Overseas Research Student Award during the tenure of this work

References

[1] Cobbs WH Jr, Burton RL. J Polym Sci 1953;X(3):275.
[2] Keller A, Lester GR, Morgan LB. Proc Roy Soc A 1954;247:1.
[3] Hartley FD, Lord FW, Morgan LB. Proc Roy Soc A 1954;247:2.
[4] Van Antwerpen F, Van Krevelen DW. J Polym Sci, Polym Phys Ed 1972;10:2423.
[5] Mehta A, Gaur U, Wunderlich B. J Polym Sci, Polym Phys Ed 1978;16:289.
[6] Gümther B, Zachmann HG. Polymer 1983;24:1008.
[7] Habarin SA. J Appl Polym Sci 1987;34:97.
[8] Mayhan KG, James WJ, Bosch W. J Appl Polym Sci 1965;9:3605.
[9] Mitsuishi Y, Ikeda M. J Polym Sci, Part A2 1966;4:283.
[10] Ozawa T. Polymer 1971;12:150.
[11] Misra A, Stein RS. J Polym Sci, Polym Lett 1972;10:473.
[12] Stein RS, Misra A. J Polym Sci, Polym Phys Ed 1973;11:109.
[13] South FS, Steward RD. Polymer 1974;15:283.
[14] Frank WP, Zachmann HG. Colloid Polym Sci 1977;62:88.
[15] Reinsch VE, Rebenfeld L. J Appl Polym Sci 1994;52:649.
[16] Jackson JB, Longman GW. Polymer 1969;10:873.
[17] Van Antwerpen F, Krevelen DW. J Polym Sci, Part C 1970;30:271.
[18] Gunter B, Zachmann HG. Polymer 1983;24:1008.
[19] Price FP. Encycl Polym Sci Technol 1968;8:63.
[20] Booth A, Hay JN. Polymer 1969;10:95.
[21] Hay JN, Mills PJ. Polymer 1982;23:1380.
[22] Van Antwerpen F, Van Krevelen DW. J Polym Sci, Polym Phys Ed 1972;10:2423.
[23] Mehta A, Gaur U, Wunderlich B. J Polym Sci, Polym Phys Ed 1978;16:289.
[24] CRC handbook of chemistry and physics. 53rd ed. USA: CRC press, 1972. p. B-241.
[25] Wunderlich B. Macromolecular physics, vol. 2 1976.
[26] Hay JN. Br Polym J 1971;3:74.
[27] Banks W, Gorden M, Roe R-J, Sharples A. Polymer 1963;4:289.
[28] Banks W, Sharples A, Hay JN. J Polym Sci 1964;A-2(2):4059.
[29] Hillier IH. J Polym Sci, Part A 1965;3:3067.
[30] Price FP. J Polym Sci, Part A 1965;3:3079.
[31] Verhoyen O, Dupret F, Legras R. Polym Engng Sci 1998;38:1594.
[32] Bell JP, Murayama T. J Polym Sci 1969;A-2(7):1059.
[33] Roberts RC. Polym London 1969;10:117.
[34] Sweet GE, Bell JP. J Polym Sci, A-2 1972;10:1273.
[35] Douillard A, Dumazet Ph, Chabert B, Guillet J. Polymer 1993;34:1702.
[36] Flory PJ. J Chem Phys 1949;17:223.
[37] Hoffman JD, Weeks JJ. J Res Natl Bur Stand 1962;A73:64.
[38] Hoffman JD, Davis GT, Lauritzen JI. In: Hannay JB, editor. Treatise on solid state chemistry: crystalline and non-crystalline solids, vol. 3. New York: Plenum Press, 1976.
[39] Chan TW, Isayev AI. Polym Engng Sci 1994;34:461.
[40] Hoffman JD, Frolen LJ, Ross GS, Lauritzen JIIr. J Res NBS 1975;79A(6):671.
[41] Plays LH, Phillips PJ. J Polym Sci 1980;18:829.
[42] Miller RL, Boyer RF. J Polym Sci, Polym Phys Ed 1977;15:1475.
[43] Daubeny R De P, Bunn CW. Proc R Soc London A 1954;226:531.
[44] Turnbull D, Cormia RL. J Chem Phys 1961;34:820.
[45] Wlochowicz A, Przygocki W. J Appl Polym Sci 1973;17:1197.